

Evolution of ferroelectric LiNbO_3 phase in a reactive glass matrix ($\text{LiBO}_2\text{--Nb}_2\text{O}_5$)

N. Syam Prasad, K.B.R. Varma *

Materials Research Centre, Indian Institute of Science, Bangalore 560 012, India

Abstract

Transparent glasses in the system $(100 - x)\text{LiBO}_2\text{--}x\text{Nb}_2\text{O}_5$ ($5 \leq x \leq 25$, in molar ratio) were fabricated by the conventional melt quenching technique. The as-quenched samples were amorphous as established via X-ray powder diffraction (XRD) studies. Differential thermal analyses (DTA) confirmed their glassy nature. The glass transition temperature (T_g) and the crystallization temperature were found to be strongly composition (x) dependent. Lithium niobate (LiNbO_3) nanocrystals were produced within the glass by heat-treating it at $500^\circ\text{C}/3\text{ h}$ (for $x = 15$). Two-stage heat-treatment process has improved the optical transmission characteristics. Impedance analysis was done to rationalize the electrical behavior of these glasses embedded with 100 nm sized LiNbO_3 crystallites. The observed pyroelectric response and ferroelectric (P vs E) hysteresis loop at room temperature confirmed the polar nature of these composites.

1. Introduction

Transparent ferroelectric glass-ceramics have been of increasing interest over the single crystals owing to their potential applications for multifunctional devices. The optical and polar properties could be appreciably changed by varying the volume fraction of the active phase dispersed and its nano/microstructure. The transparent composites embedded with ferroelectric crystals could be tailored to exhibit either Kerr or Pockels effects depending on the crystallite size. Yet another important factor is that these could be obtained with relative ease. These are also of technological prominence because of the flexibility that this route offers in fabricating into intricate sizes and shapes depending on the requirement. A number of glass-ceramics comprising well-known fer-

roelectric crystalline phases (BaTiO_3 , LiNbO_3 , LaB_5GeO_5 , $\text{Sr}_{0.5}\text{Ba}_{0.5}\text{Nb}_2\text{O}_6$, $\text{SrBi}_2\text{Nb}_2\text{O}_9$, etc.) have been fabricated and investigated for their polar and electro-optic properties [1–6].

Single crystals of Lithium Niobate (LiNbO_3) are important non-linear optic (NLO) materials because of their efficient second harmonic generation (SHG) as well as high electro-optic and elasto-optic coefficients [7–9]. It is because of these promising properties, LiNbO_3 has occupied a prominent place in the fabrication of optical waveguides, modulators, switches and optical circuits [10]. Keeping these applications in view, many researches around the globe have been making attempts to fabricate transparent glasses comprising LiNbO_3 crystallites. As a first attempt Imaoka and Yamazaki [11] reported the glass-forming region in the system $\text{TeO}_2\text{--Li}_2\text{O}\text{--Nb}_2\text{O}_5$. Komatsu et al. [3] fabricated transparent telluride glasses containing ferroelectric LiNbO_3 crystals. In crystallizing ferroelectric LiNbO_3 phase in these glasses, one invariably encounters an intermediate

* Corresponding author. Tel.: +91 80 309 2914; fax: +91 80 360 0683.
E-mail address: kbrvarma@mrc.iisc.ernet.in (K.B.R. Varma).

pyrochlore phase precipitating during the heat-treatment [3,12]. However, the direct crystallization of LiNbO₃ was achieved in telluride glasses with high Li content through a two-stage heat-treatment [13]. The surface crystallization of LiNbO₃ in the TeO₂–LiNbO₃ glass system was demonstrated by one of the authors through single-stage heat-treatment [14].

The event of the pyrochlore and centrosymmetric LiNb₃O₈ impurity phase formation along with the desired LiNbO₃ in TeO₂ glass matrix is a nuisance in achieving monophasic transparent LiNbO₃ phase. Recently, transparent LiNbO₃ glass–ceramics were fabricated in the crystallization of LiNbO₃–SiO₂–Al₂O₃ glass system [15,16]. In all the processes, that were reported so far in the literature, either pre reacted LiNbO₃ or constituent oxides were taken in suitable ratios and recrystallized or allowed to react in glass matrices wherein it was difficult to exercise strict control over the crystallite size which is very crucial for obtaining transparent glass–ceramics especially in optically incompatible glass matrices. Therefore, we thought it was worth attempting to crystallize the desired phase as a result of the in situ chemical reaction. For this purpose we have chosen LiBO₂ as the matrix, which is rich in Li (as compared to the other borates known in the literature) which is essential to overcome the formation of impurity phase, LiNb₃O₈. We were successful in preparing the LiBO₂–Nb₂O₅ glasses in a binary system with different compositions from which transparent LiNbO₃ crystallites were grown as a result of the reaction between Li and Nb₂O₅.

In this paper, we report the results concerning the glass formation and evolution of the nanocrystalline LiNbO₃ phase in the glass system (100 – x)LiBO₂– x Nb₂O₅ ($5 \leq x \leq 25$, in molar ratio). The structural, microstructural, ferroelectric, pyroelectric and dielectric characteristics of the glass composite, embedded with LiNbO₃ nanocrystals, are elucidated.

2. Experimental

Glasses in the system (100 – x)LiBO₂– x Nb₂O₅ ($5 \leq x \leq 25$, in molar ratio) were prepared by conventional melt quenching technique. All the glasses under investigation were prepared from reagent grade LiBO₂ and Nb₂O₅. Well mixed batches were melted in a platinum crucible at 1100–1250 °C for 1 h to yield 15 g of the glass. Melts were quenched by pouring on a steel plate that was maintained at 150 °C (to prevent the glass samples from cracking) and pressed with another plate to obtain 1–1.5 mm thick glass plates. Subsequently all the samples under study were heat-treated at 300 °C for 6 h, well before glass transition temperature (T_g) to anneal out thermal stresses that are likely to be associated with them.

The glassy nature of the as-quenched samples was established by subjecting them to differential thermal analyses (DTA) in the 30–800 °C temperature range. A uniform heating rate of 15 °C/min was adopted for this purpose. Three samples of each composition were subjected to DTA and the average value of the glass transition (T_g) and crystallization temperatures (T_{cr}) were determined. X-ray diffraction studies were performed at room temperature on the as-quenched and heat-treated samples at different temperatures to confirm their amorphous and crystalline nature respectively. Transmission electron microscope (TEM) was employed for electron diffraction and high-resolution electron microscopic studies on the as-quenched and heat-treated samples. Microstructural analyses on the heat-treated samples were done by using scanning electron microscope (SEM).

The capacitance and impedance (Z' and Z'') measurements on both the as-quenched and heat-treated (500 °C/3 h) samples were done using an impedance gain phase analyzer in the frequency range 100 Hz–40 MHz with a signal strength of 0.5 V rms at various temperatures (300–600 °C). For this purpose polished samples were gold electroded and thin copper leads were bonded using the silver epoxy. The samples were held at fixed temperatures for a few minutes before making the measurement. Complex impedance plots were generated for the as-quenched and heat-treated samples at different temperatures. The low frequency intercept of the semicircle on the x -axis is considered to be the bulk resistance (R_b). The bulk capacitance (C_b) was calculated by considering the condition $2\pi f_0 R_b C_b = 1$, where f_0 , relaxation frequency is the frequency maximum in the semicircle and R_b is the bulk resistance.

Pyroelectric current measurements were carried out as a function of temperature by employing the direct method due to Byer and Roundy [17] using a auto-ranging picoammeter in conjunction with a programmable temperature controller. Ferroelectric hysteresis loop measurements were performed at a switching frequency of 50 Hz using a modified Sawyer–Tower circuit. The values of remanent polarization (P_r) and the coercive field (E_c) were determined from the hysteresis loop. Prior to the pyroelectric and ferroelectric measurements, all the samples under study were electrically poled at different fields using an indigenously built DC power supply in the 150–250 °C temperature range.

The optical transmission spectra of the as-quenched polished and heat-treated samples (glass nanocomposites) were recorded in the 200–900 nm wavelength range using an Hitachi U3000 spectrophotometer. The absorption coefficient (α), calculated based on the Beer Lambert's law is employed to evaluate the optical band gap energy (E_g) by the Tauc's equation.

$$\alpha h\nu = m(h\nu - E_g)^2,$$

where h is the Planck constant, ν is the frequency of radiation and m is a constant proportional to the joint density of states. The optical band gap energy (E_g) was calculated from the Tauc plot of $(\alpha h\nu)^{1/2}$ vs photon energy ($E = h\nu$).

Birefringence (Δn) of the glass nanocomposites was measured by the method described below. P-polarized laser beam from argon ion laser (Uniphase 2011) was allowed to pass through the sample via an aperture and a converging lens. The output light beam from the sample was allowed to pass through an analyzer kept in crossed condition with the polarized laser beam. The output from the analyzer was detected by a photo multiplier tube and read by a high precession digital multimeter. The output beam intensity was monitored at 515 nm wavelength of the laser at different sample temperatures. The intensity of the light emerging out of the analyzer when it was kept in crossed condition with the input polarized laser beam, along with the sample could be written as

$$I = I_0 \sin^2 \left(\frac{\pi \Delta n d}{\lambda} \right),$$

where I_0 is the initial intensity of the laser beam in the absence of the sample and the analyzer. Δn is the birefringence to be determined and d the thickness of the sample. λ is the wavelength of the laser light used.

3. Results and discussion

Transparent colorless glasses, of varied dimensions without any visible inclusions were fabricated in the system $(100 - x)\text{LiBO}_2 - x\text{Nb}_2\text{O}_5$ ($5 \leq x \leq 25$, in molar ratio). Glasses of compositions higher than $x = 25$ could not be quenched into glasses. Therefore the present investigations have been confined to the compositions which fall within the glass-forming region.

3.1. Thermal studies

The DTA curves that were obtained for the as-quenched glass pieces corresponding to the representative compositions $x = 5, 10, 15, 20$ and 25 are shown in Fig. 1(a)–(e). A major exothermic event along with less intense ones are observed for all the as-quenched samples except for $x = 10$. The samples heat-treated at the onset temperatures of the major exothermic peaks did not exhibit these peaks on subsequent DTA studies, indicating their crystalline nature. DTA studies (not described here) carried out on the samples with higher concentrations ($x = 30$ and above) did not reveal any exo/endothermic events before melting, suggesting the crystalline nature of the as-quenched samples.

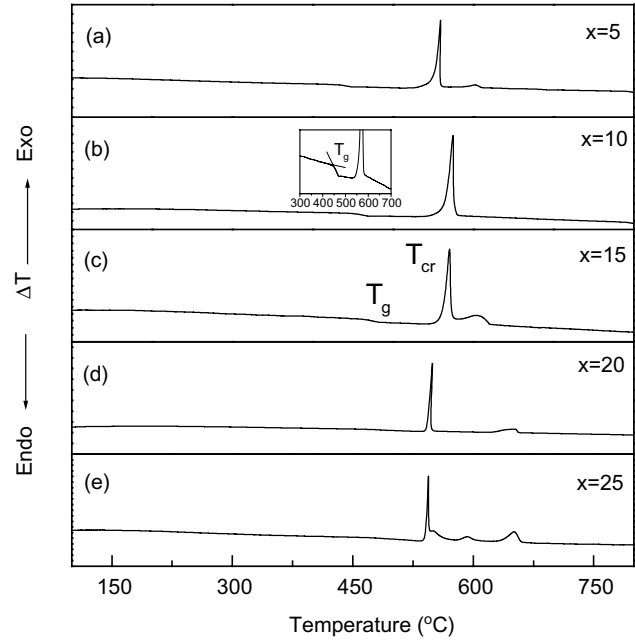


Fig. 1. Differential thermograms for the as-quenched samples.

Fig. 2 shows the compositional dependence of the glass transition temperature (T_g), crystallization temperature (T_{cr}) and the thermal stability (ΔT). It is observed that the glass transition temperature increases with the increase in the composition x , while the crystallization temperature initially increases until the composition corresponding to $x = 10$ and subsequently it decreases with increase in x . The estimated thermal stability of these glasses against crystallization based on Dietzel criterion, $\Delta T = T_{cr} - T_g$, is found to decrease with increase in the Nb_2O_5 content (x). The increase in T_g is ascribed to a decrease in the number of non-bridging oxygens as the amount of LiNbO_3 crystalline phase increases. It is

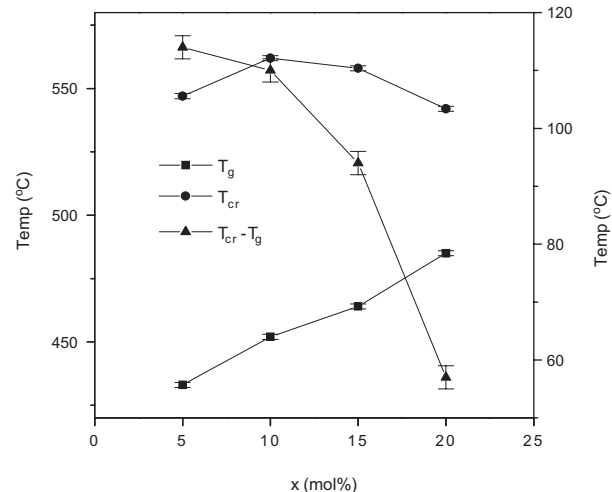


Fig. 2. Compositional variation of glass transition temperature (T_g), crystallization temperature (T_{cr}) and the thermal stability ($T_{cr} - T_g$).

due to the fact that as the Nb_2O_5 content increases in LiBO_2 , it scavenges more Li ions as a consequence the number of non-bridging oxygens decreases. In order to evaluate the phase which is associated with the exothermic peaks in DTA studies, a systematic XRD analyses have been carried out on the heat-treated samples of different compositions.

3.2. XRD studies

The X-ray powder diffraction (XRD) patterns of the as-quenched glasses corresponding to the composition $(100 - x)\text{LiBO}_2 - x\text{Nb}_2\text{O}_5$ (where $x = 5$ and 20) confirm their amorphous nature (Fig. 3(a) and (b)). The XRD patterns recorded for the samples ($x = 5, 10, 15$ and 20) heat-treated in the vicinity of first exotherm ($\approx 500^\circ\text{C}$) are shown in Fig. 3(c)–(f). The d -spacings that are associated with these patterns are in good agreement with those reported in the literature for a polycrystalline LiNbO_3 phase obtained by the conventional solid state reaction route [17]. The lattice parameters ($a = b = 5.149$ and $c = 13.846 \text{ \AA}$) computed based on the present data are indeed in close agreement with those ($a = b = 5.1494$ and $c = 13.862 \text{ \AA}$) reported in the literature for LiNbO_3 . XRD recorded for the composition $x = 20$ (Fig. 3(f)), shows Bragg reflections at $2\theta = 21.45$ and 30.15 in addition to the LiNbO_3 reflections. The d -spacings that are associated with these reflections are

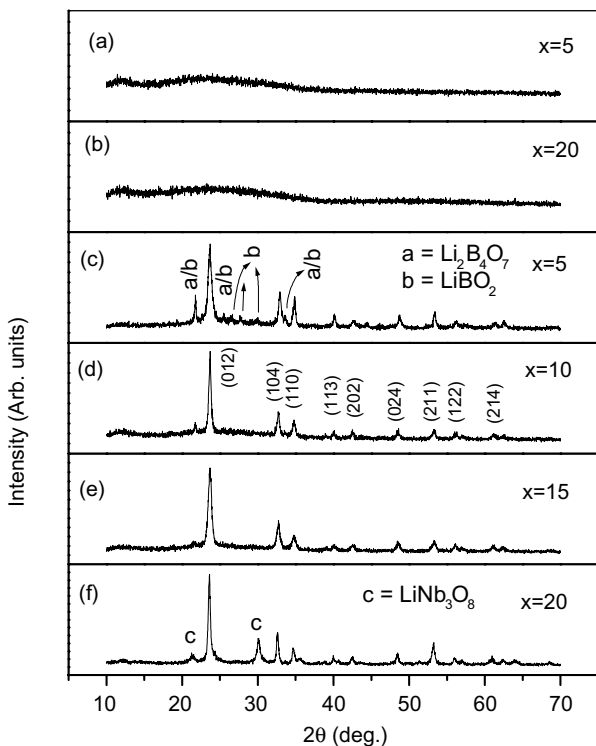


Fig. 3. XRD patterns for the as-quenched (a,b) and the sample heat-treated at $500^\circ\text{C}/3\text{ h}$ (c)–(f).

in good agreement with the intense peaks reported for a centrosymmetric LiNb_3O_8 phase [18]. It is also observed that the intensity of the peaks corresponding to the LiNb_3O_8 phase formation increases with increase in the Nb_2O_5 composition ($x \geq 20$). For lower values of x ($x = 5$), apart from the presence of the major LiNbO_3 phase, we did observe low intense peaks ($2\theta = 21.75$ and 25.39) (Fig. 3(c)) corresponding to the LiBO_2 and $\text{Li}_2\text{B}_4\text{O}_7$ phases. It implies that apart from major LiNbO_3 phase, the matrix has crystalline LiBO_2 and $\text{Li}_2\text{B}_4\text{O}_7$ phases.

3.3. TEM studies

Transmission electron micrographs along with the selected area electron diffraction (SAED) patterns recorded for the as-quenched and heat-treated (500°C) samples of the representative composition $x = 15$ are shown in Fig. 4. The diffraction pattern (Fig. 4(a)) that is obtained for the as-quenched glass indicates its amorphous nature. However the presence of nearly sharp spherical rings around the bright central region suggests the presence of local ordered regions. Fig. 4(b) shows a bright field image obtained for the sample obtained by two-stage heating ($460^\circ\text{C}/6\text{ h}$ and $500^\circ\text{C}/3\text{ h}$) which indicates a fine distribution of spherical crystallites in the glass matrix. The average crystallite size is found to be $25 (\pm 6)$ nm. The d -spacings obtained based on the selected area electron diffraction (SAED) pattern are $3.70, 2.70, 2.34, 2.21, 1.89, 1.76, 1.69$ and 1.51 \AA . These are in good agreement with those reported for the LiNbO_3 phase. Fig. 4(c) shows the TEM obtained for the samples heat-treated at $500^\circ\text{C}/3\text{ h}$ (single stage). The average crystallite (acicular) size is found to be $100 (\pm 14)$ nm.

3.4. SEM studies

SEM was done to visualize the microstructural changes that follow, on increasing the heat-treatment temperature. Fig. 5 shows the scanning electron micrographs recorded for the samples of the composition $85\text{LiBO}_2 - 15\text{Nb}_2\text{O}_5$ ($x = 15$) heat-treated at different temperatures. Fig. 5(a) which is recorded for the sample heat-treated at 475°C (which is above the nucleation temperature (T_n)), reveal the formation of phase separated regions on a finer scale and appear to coalesce on further heating. The phase separated regions evidently suggest that the nucleation and growth process could be responsible for the development of this kind of microstructure. Scanning electron micrograph recorded for the sample heat-treated at 500°C (Fig. 5(b)) shows a spread in these regions and appear nearly spherulitic. Though the size of the spherulite is in the range of $20\text{--}30 \mu\text{m}$, the size of the LiNbO_3 crystallites is only few nm. SEM recorded for the samples

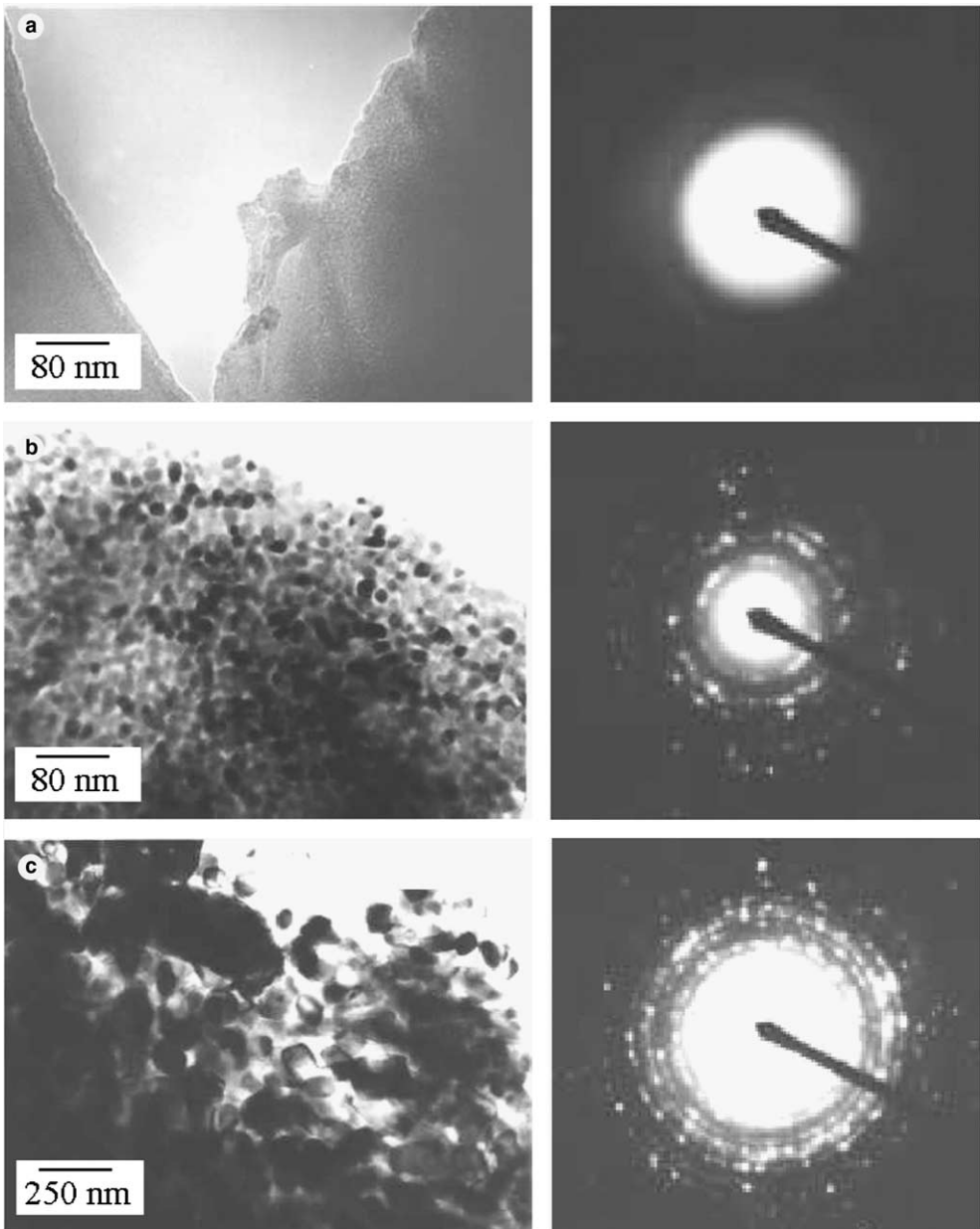


Fig. 4. Transmission electron micrographs along with the SAED patterns recorded for the (a) as-quenched, (b) 460 °C/3 h and 500 °C/3 h and (c) 500 °C/3 h heat-treated glasses of the composition $x = 15$.

heat-treated at 600 °C and 650 °C are shown in Fig. 5(c) and (d) respectively. The sample heat-treated at 600 °C shows the presence of nearly 0.3 (± 0.1) μm sized crystallites evolved from the glass matrix. These crystallites are found to grow further when the sample is heat-treated to 650 °C/3 h. Nevertheless, the samples heat-treated at higher temperatures (>500 °C) revealed the presence of voids/micro cracks as depicted in the inset of Fig. 5(c). With increase in heat-treatment temperature the volume percentage and the connectivity of these voids/micro cracks are found to increase and resulted in low density composites which are not favorable for electrical applications as they were found more leaky than the samples

without voids (samples heat-treated at 500 °C). The void/micro crack formation in the samples heat-treated at higher temperatures is attributed to the thermal expansion mismatch to a considerable extent in the crystalline phases involved.

The density measurements carried out for the samples heat-treated at different temperatures for all the compositions are listed in Table 1. The density is observed to increase with increase in the Nb_2O_5 composition (x) as a consequence of the presence of higher volume fraction of the dense LiNbO_3 . The samples heat-treated at 500 °C show higher densities than those of the as-quenched samples and those heat-treated at 600 °C. This

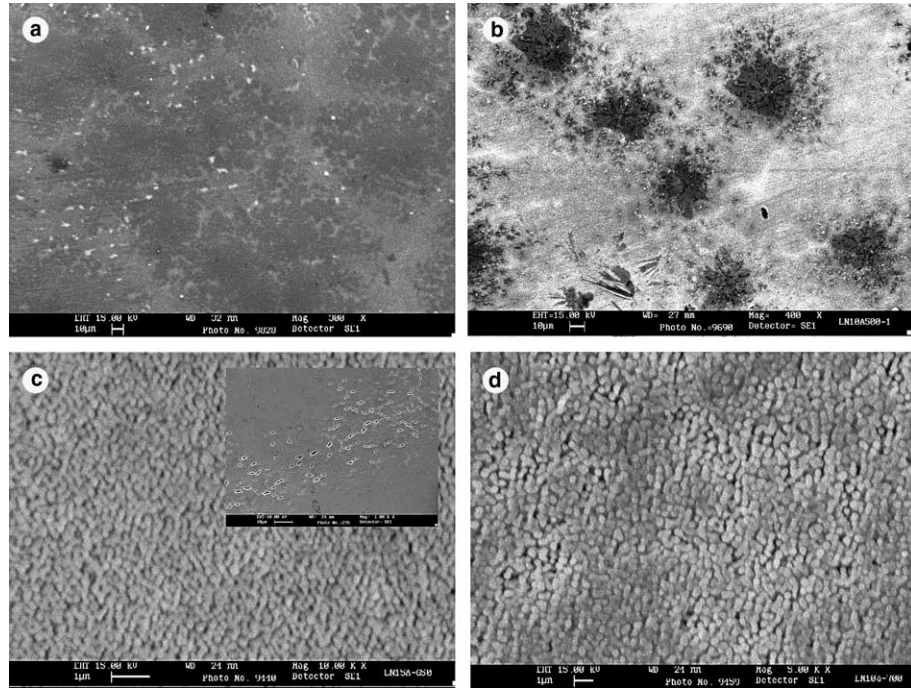


Fig. 5. SEM recorded on the samples heat-treated at (a) 470 °C, (b) 500 °C, (c) 600 °C and (d) 650 °C of the composition $x = 15$. Inset of (c) shows voids/micro crack formation.

Table 1
Compositional variation of densities measured on the samples heat-treated at different temperatures

Nb_2O_5 composition (x)	Density (g/cc) measured at different heat-treatment temperatures		
	300 °C	500 °C	600 °C
5	2.570	2.666	2.613
10	2.832	2.962	2.821
15	2.917	3.208	3.097
20	3.197	3.440	3.321

could be attributed to the void/micro crack formation as observed in SEM analyses.

3.5. Optical properties

The samples obtained by one-stage heat-treatment at 500 °C/3 h (close to the first exothermic peak observed in DTA) are found to have lower levels (20% at 700 nm) of transparency. In order to improve the transparency, which is linked with the nucleation, growth and the size of crystallites embedded in the glass matrix a two-stage heat-treatment procedure has been adopted. Two-stage heat-treatment process in which the as-quenched samples were heated to 460 °C/3 h (first heating) followed by 500 °C/3 h (second heating). Thus obtained samples were observed to have improved transmission (50% at 700 nm) characteristics than those obtained by single-stage heat-treatment. The reason for choosing 460 °C as a first heating stage is based on our

earlier studies [19] on nucleation and growth in which the maximum nucleation rate was found to be around 460 °C. The maximum number of nuclei that occurred at 460 °C on subsequent heating at 500 °C hinder grain growth which facilitates better transmission. The increase in the crystallite size in the matrix which has a refractive index lower than that of LiNbO_3 crystallites would not allow the light to transmit as a consequence of large scattering at the crystal–glass interfaces.

The optical transmission was recorded for all the as quenched and heat-treated (at 500 °C/3 h) samples in the wavelength range 200–900 nm. Fig. 6 shows the transmission spectra for the LiBO_2 glass, the as quenched and heat-treated (at 500 °C/6 h) glasses of the composition $x = 15$. In the case of pure LiBO_2 and the as-quenched glass of the composition $x = 15$, the percentage transmission is nearly constant in the 900–300 nm range. The transmission suddenly drops and reaches almost zero below 300 nm. The sample heat-treated at 500 °C (one-stage heating) shows very poor transmission characteristics. However the sample prepared by two-stage heat-treatment exhibits improved transmission characteristics. The optical absorption edge (wavelength at which the percentage transmission is zero; $\lambda_{\text{cut-off}}$) that is encountered in the present studies (375 nm) is in agreement with the values reported for the transparent LiNbO_3 glasses [14,20]. The $\lambda_{\text{cut-off}}$ shifts towards longer wavelengths (red shift) for the heat-treated sample. Similar shift has been observed with increase in Nb_2O_5 content. Optical band gap (E_g) was calculated from the Tauc plot ($(\alpha h\nu)^{1/2}$ vs $h\nu$) generated based on

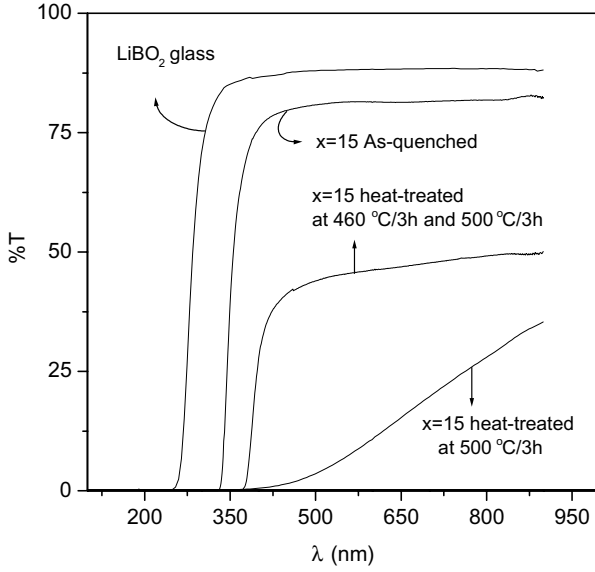


Fig. 6. The optical transmission spectra for LiBO₂ glass and the as-quenched and heat-treated glasses of the composition 85LiBO₂–15Nb₂O₅.

the transmission data. Typical Tauc plots for the as-quenched and heat-treated samples of the composition $x = 15$ are shown in Fig. 7. Transparent nature of the glasses containing nanocrystallites of LiNbO₃ prompted us to measure the SHG. The preliminary work that was carried out with regard to the establishment of non-centrosymmetric nature of these composites using SHG study as a tool yielded interesting results. The detailed investigations have been in progress and the full details of this work along with micro Raman studies will be reported shortly.

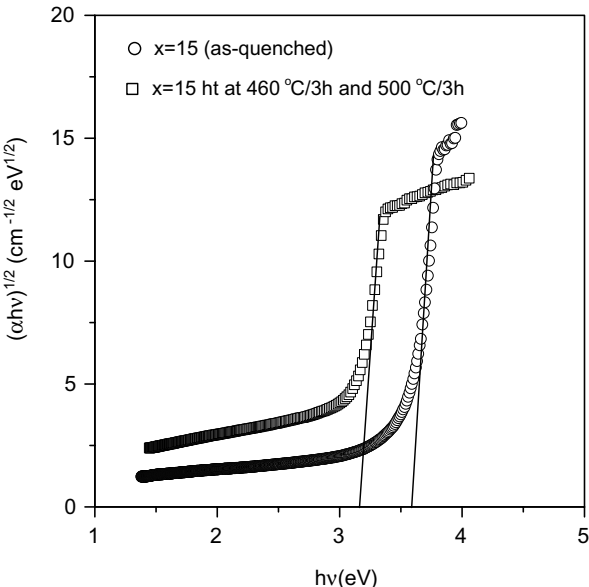


Fig. 7. The variation of the $(\alpha h\nu)^{1/2}$ with $h\nu$.

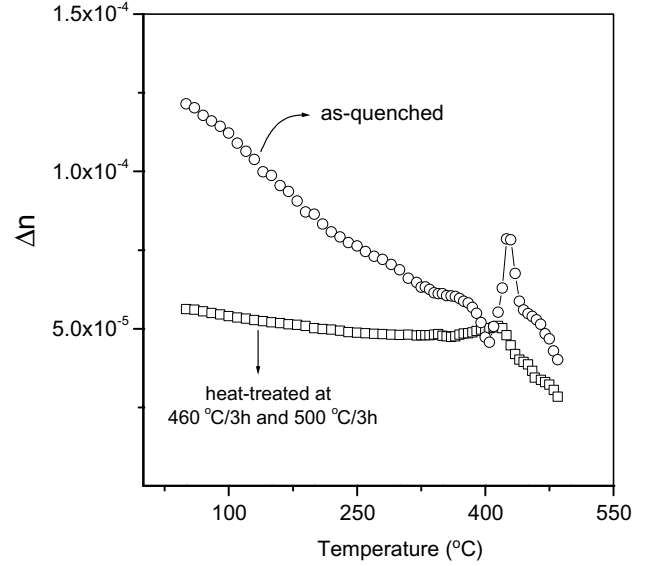


Fig. 8. Temperature variation of birefringence for as-quenched and heat-treated samples of the composition $x = 15$.

As-quenched and 500 °C (two-stage heat-treated) glasses are found to be birefringent. All the samples under study exhibit this nature, but the value Δn is observed in case of the heat-treated samples to be very small as compared to the single crystalline LiNbO₃. This can be attributed mainly to the small size of the crystallites and their random orientation. Temperature variation of the birefringence of the glass and glass nanocomposite (two-stage heat-treated) of the composition $x = 15$ is shown in Fig. 8. At room temperature as-quenched sample show higher value of Δn than the heat-treated sample of the same composition. This can be ascribed to the stress birefringence, which is very common in the as-quenched glasses [21]. This contribution would be minimal in the case of heat-treated samples as heat-treatment lowers the stress associated with the sample. In both the cases Δn is found to decrease till 400 °C and exhibits a small anomaly around 500 °C and decreases to a minimum at 550 °C. This is due to the opaque nature of the sample which results in zero transmitted light [22], because of the excessive growth of LiNbO₃ and the scattering of light due to a significant difference in refractive indices between LiNbO₃ and LiBO₂ glass matrix.

3.6. Dielectric studies

The frequency response of the dielectric constant (ϵ_r) along with that of dielectric loss (D) were monitored for all the glass nanocomposites i.e. the glasses heat-treated at 500 °C. Fig. 9 shows a typical plot obtained for the composition 85LiBO₂–15Nb₂O₅. The dielectric constant as well as the dielectric loss decrease rapidly in the low frequency region up to about 10 kHz and subsequently

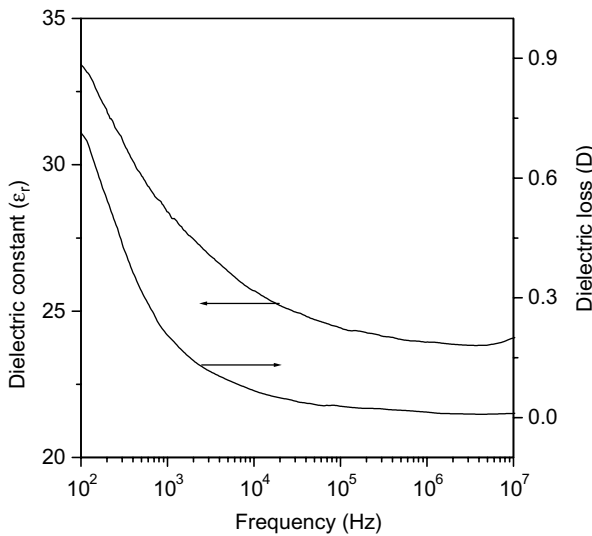


Fig. 9. Frequency response of dielectric constant (ϵ_r) and dielectric loss (D) for the $85\text{LiBO}_2\text{-}15\text{Nb}_2\text{O}_5$ glass nanocomposite heat-treated at $500\text{ }^\circ\text{C}/3\text{ h}$.

the dispersion with frequency is insignificant. The decrease in both ϵ_r and D for glass nanocomposite with increase in frequency could be explained by using Stevles and Taylor model, which was proposed to understand the dielectric relaxation and ionic conductivity behavior of alkali silicate glasses [23,24]. In vitreous substances as these are disordered at molecular level, one would expect a variation in the free energy barriers from site to site in the quasi lattice unlike in a material with a long range lattice structure. Ions under dc or low frequency conditions can hop readily out of sites with low free energy barriers in the direction of the applied electric field but tend to ‘pile up’ at sites with high free energy barriers. This leads to a net polarization of the ionic medium and hence a large contribution to the low frequency value of ϵ_r . At high frequencies the polarization due to charge ‘pile up’ at high free energy barriers disappears which results in the decrease of ϵ_r .

The dielectric constant (ϵ_r) and the dielectric loss (D) measurements were carried out on different compositions in the system $(100 - x)\text{LiBO}_2\text{-}x\text{Nb}_2\text{O}_5$ ($5 \leq x \leq 25$, in molar ratio). Measurements have been done on the glass samples heat-treated at $500\text{ }^\circ\text{C}$ which contain 100 nm sized LiNbO_3 crystallites. The dielectric constant increases with increase in Nb_2O_5 content (Fig. 10). Interestingly the dielectric loss decreases with increase in x . The increase in the dielectric constant with increase in x can be attributed to the increase in the volume fraction of high dielectric constant LiNbO_3 phase. The decrease in the dielectric loss with increasing x is ascribed to the hindrance in the motion of Li^+ ions, caused by the presence of inter penetrating glass–crystallite interfaces.

The variation of dielectric constant as a function of temperature at 1 kHz for the as-quenched and heat-

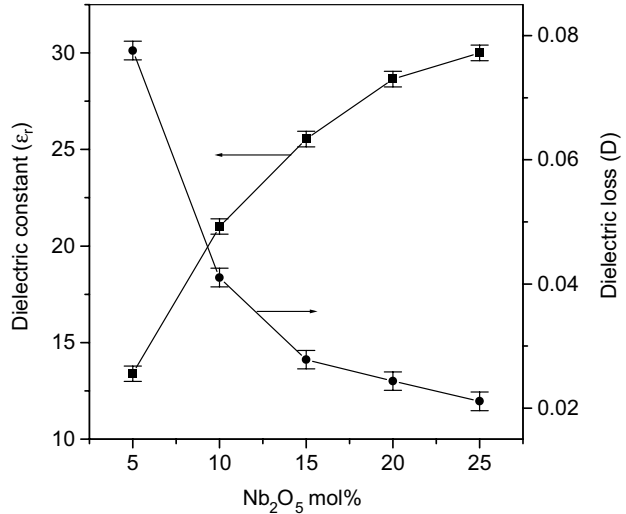


Fig. 10. Variation of the dielectric constant (ϵ_r) and dielectric loss (D) as a function of Nb_2O_5 content for $500\text{ }^\circ\text{C}/3\text{ h}$ heat-treated glasses in the system $(100 - x)\text{LiBO}_2\text{-}x\text{Nb}_2\text{O}_5$.

treated ($500\text{ }^\circ\text{C}/3\text{ h}$) samples is shown in Fig. 11. It is observed that the dielectric constant of the sample heat-treated at $500\text{ }^\circ\text{C}$ is higher than the value obtained for the as-quenched glass at room temperature. In both the cases the dielectric constant is found to increase with increase in the temperature. As-quenched sample showed anomaly in the vicinity of the crystallization temperature, which is consistent with the DTA studies. The sample heat-treated at $500\text{ }^\circ\text{C}$ also showed similar trend but the observed magnitude is found to be very small. This suggests the crystallization of residual glass in the heat-treated samples. The incidence of dielectric anomaly is due to the conduction-related polarization

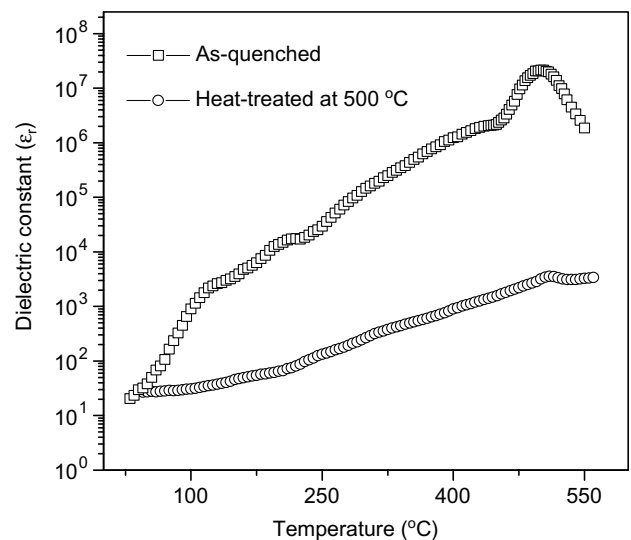


Fig. 11. Temperature variation of the dielectric constant for the as-quenched and heat-treated ($500\text{ }^\circ\text{C}/3\text{ h}$) glasses of the composition $x = 15$.

in the glasses. Several models have been proposed concerning conduction-related polarization in alkali silicate glasses, which are more or less applicable to alkali borate glass systems [25,26]. Charles assumed that there are a number of available sites for an alkali ion around a non-bridging oxygen ion. Doi suggested that the conduction proceeds through sequential steps [27]. These motions give rise to conduction polarization, which could be termed as orientational polarization of the alkali-non-bridging oxygen pseudo-dipoles. At the crystallization temperature the ions indulge in rapid movement to transform from a random or glassy to ordered crystalline state and hence the higher dielectric constant via higher conduction-related polarization. The dielectric maximum observed at the crystallization temperature could be partly due to the maximum in conduction-related polarization, in the temperature region of glass crystallization.

3.7. Impedance analyses

Impedance spectroscopy is one of the useful techniques employed to rationalize the electrical behavior of dielectrics. We wanted to visualize the effectiveness of impedance spectroscopy for the characterization of nanocrystallites of LiNbO_3 in LiBO_2 glass matrix. In the complex impedance plot, the semicircle at high frequency end represents the grain interior, the second semicircle shows the grain boundary response and the third one at low frequency side indicates the electrode-sample interface effects.

The impedance plots (Z' vs Z'') at various temperatures for the heat-treated (500°C) glass composites of the composition $x = 15$ are shown in Fig. 12. The occurrence of a single semicircle in the present studies

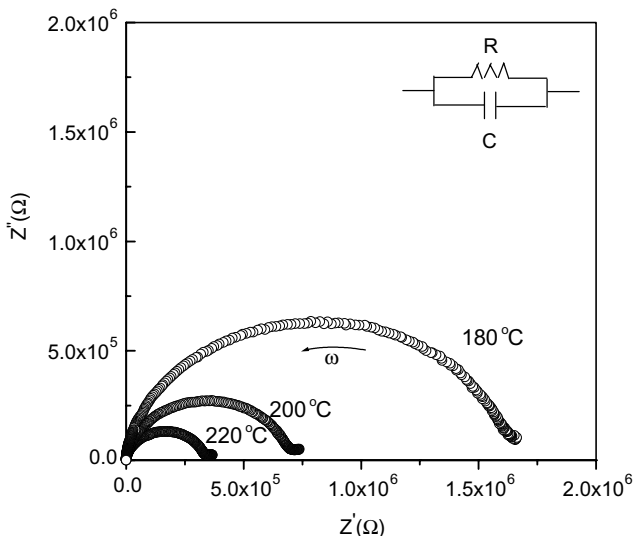


Fig. 12. Complex impedance plots at various temperatures for the glass nanocomposite (heat-treated at $500^\circ\text{C}/3\text{ h}$) of the composition $x = 15$.

indicates the AC response of the nanosized LNB crystallites embedded in the LBO host glass matrix. This implies that it could be represented by a single parallel RC element. TEM studies on the composites evidently corroborate the presence of $\cong 100\text{ nm}$ LNB crystallites, which are separated by the glassy regions of the host matrix. This is analogous to that of grains and grain boundaries in a polycrystalline material except for the presence of glassy material at the grain boundaries. In the present case the intercept of the semicircle with the x -axis on the lower frequency side is referred as the bulk resistance (R_b) of the sample. It is considered to be the resistance of the LNB nanocrystallites dispersed in the glass matrix. The intercept of the semicircle on the x -axis shifts towards lower values of Z' with increase in temperature of the measurement, indicating a decrease in the bulk resistance of the samples. Table 2 indicates the values of bulk resistance (R_b), relaxation frequency (f_0) and the calculated bulk capacitance (C_b). It is observed that the R_b values evaluated for the sample under study are less than the values reported for pure LiNbO_3 ceramic [28], which is attributed to the nanosized crystallites. The activation energy that is computed based on the Arrhenius formula (Fig. 13) is found to be 0.74 eV. The temperature dependence of the relaxation frequencies also follow the same trend (Fig. 13) as that of the electrical conductivity.

3.8. Pyro- and ferroelectric properties

The structural evidence of the presence of fine crystallites of LiNbO_3 grown in LBO glass matrix encouraged us to examine these glass-ceramics for their polar properties. The pyroelectric and ferroelectric studies have been carried out on the representative composition $85\text{LiBO}_2\text{-}15\text{Nb}_2\text{O}_5$ heated at 500°C . The variation of pyroelectric coefficient (P) as a function of temperature for the sample heat-treated at 500°C is shown in Fig. 14. It is found to increase with increase in temperature. The pyroelectric coefficient observed at room temperature is $1.6\text{ }\mu\text{C/m}^2\text{ }^\circ\text{C}$. Though this value is very small as compared to the value obtained for single crystalline LiNbO_3 , it is in the range of values obtained for other polar glass-ceramic samples reported in the literature [29].

Table 2
Bulk resistance (R_b), relaxation frequency (f_0) and bulk capacitance (C_b) of glass nanocomposite (heat-treated at $500^\circ\text{C}/3\text{ h}$)

T ($^\circ\text{C}$)	R_b (Ω)	f_0 (Hz)	C_b (F)
180	1.67×10^5	5.28×10^3	1.80×10^{-11}
220	3.43×10^5	2.40×10^4	1.93×10^{-11}
260	9.34×10^4	7.43×10^4	2.29×10^{-11}
300	3.47×10^4	2.53×10^5	1.81×10^{-11}
340	1.23×10^3	7.34×10^5	1.77×10^{-11}
380	4.92×10^3	1.81×10^6	1.79×10^{-11}
420	2.20×10^3	4.05×10^6	1.79×10^{-11}

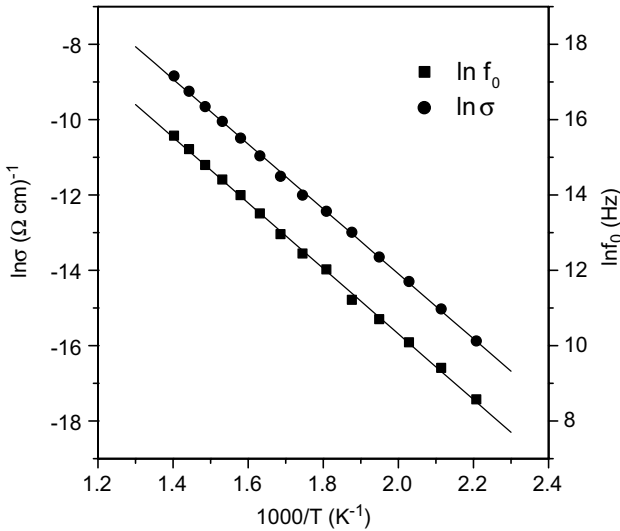


Fig. 13. Temperature dependence of electrical conductivity and relaxation frequency for the glass nanocomposite of the composition 85LiBO₂-15Nb₂O₅.

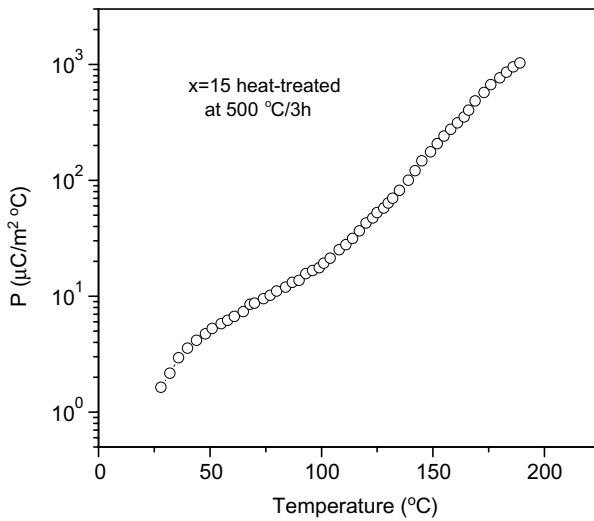


Fig. 14. Variation of Pyroelectric coefficient with temperature for the glass nanocomposite (heat-treated at 500 °C/3 h) of the composition 85LiBO₂-15Nb₂O₅.

These samples exhibited moderately good hysteresis loops between polarization and electric field right from the room temperature confirming the ferroelectric nature of the heat-treated samples. Fig. 15(a) and (b) are the loops recorded at 25 °C and 150 °C for the samples heat-treated at 500 °C of the composition $x = 15$. The value of P_r and E_c at 25 °C are 0.001 $\mu\text{C}/\text{cm}^2$ and 170 V/cm, where as the P_r and E_c at 150 °C are 11.7 $\mu\text{C}/\text{cm}^2$ and 70 V/cm respectively. These values of E_c have been very interesting as these are very much less than that reported for single crystalline LiNbO₃ at 200 °C [30]. It should be noted here that apart from the major LiNbO₃ phase present in the matrix we have

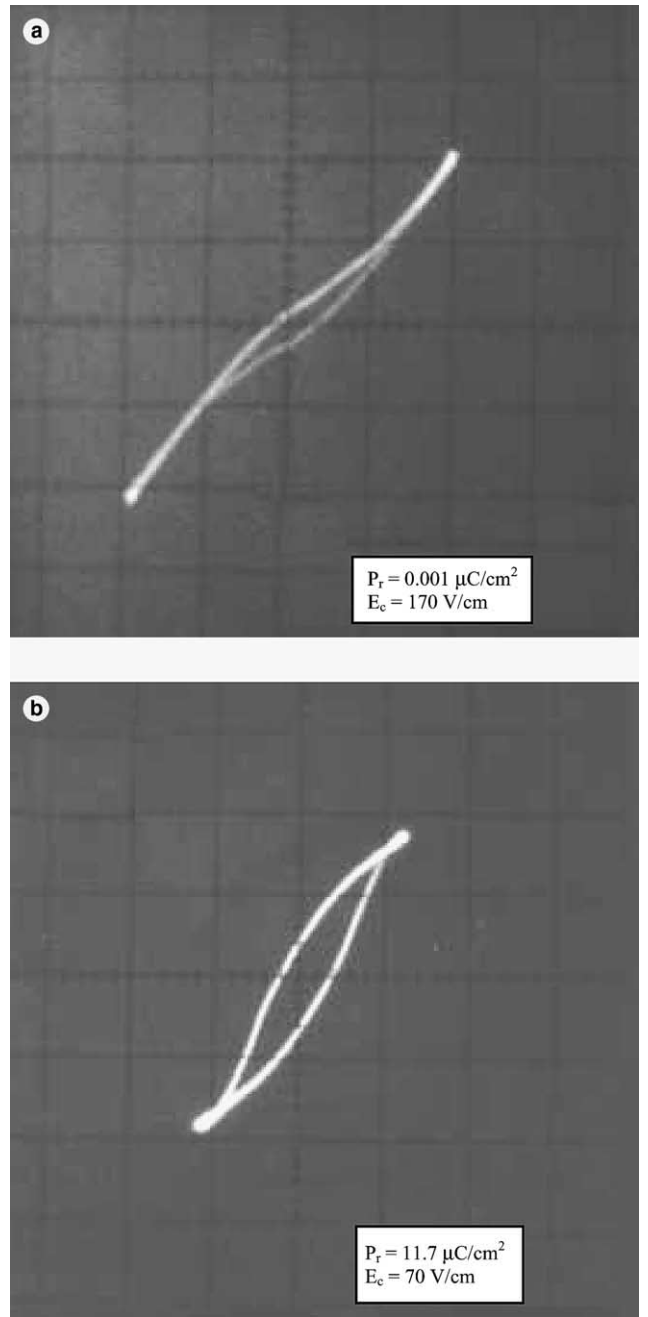


Fig. 15. $P-E$ hysteresis loops recorded on the glass nanocomposite (heat-treated at 500 °C/3 h) of the composition $x = 15$ at two different temperatures (a) 25 °C and (b) 150 °C.

Li₂B₄O₇ crystalline phase, which is reported to be ferroelectric at room temperature with $P_r = 1.44 \mu\text{C}/\text{cm}^2$ and $E_c = 2.5 \text{ kV}/\text{cm}$ [31]. In pure LiNbO₃ it was reported that for domain reversal to occur, the lithium ions have to pass through an adjacent oxygen triangle in the close packed oxygen plane. At room temperature the radius of the oxygen triangle is less than the ionic radius of lithium and as a result switching is difficult. In the present case it is likely that Li ions, which are relatively more mobile may facilitate switching of polarization at

room temperature. Apart from switching that is originated from LiNbO_3 , there could be a contribution from the presence of polar $\text{Li}_2\text{B}_4\text{O}_7$ crystallites to the observed ferroelectric characteristics of the present composite. Though we need to carry out more in depth investigations to rationalize the present data, we conjecture at this stage of research that these materials could be classified as soft ferroelectrics.

4. Conclusions

Nanocrystallization of LiNbO_3 has been demonstrated in a reactive glass system $\text{LiBO}_2\text{--Nb}_2\text{O}_5$. Compositional dependence of dielectric properties of these glass nanocomposites indicates an increase in LiNbO_3 volume fraction with increase in Nb_2O_5 content. Based on the crystallization kinetic studies, two-stage heating technique has been employed and achieved the improvement in optical transmission characteristics. The most interesting aspect of the present investigations has been the observation of pyroelectric and ferroelectric phenomena at room temperature in glass nanocomposites containing 0.1 μm sized crystallites of LiNbO_3 .

Acknowledgments

The authors thank the Council of Scientific and Industrial Research (CSIR), Government of India for financial grant. One of the authors (Syam Prasad N.) also acknowledges the University Grants Commission (UGC), Government of India, for a research fellowship.

References

- [1] N.F. Borrelli, J. Appl. Phys. 38 (1967) 4243.
- [2] A.M. Glass, M.E. Lines, K. Nassau, J.W. Shiever, Appl. Phys. Lett. 31 (1977) 249.
- [3] T. Komatsu, H. Tawarayama, H. Mohri, K. Matusita, J. Non-Cryst. Solids 135 (1991) 105.
- [4] V.N. Sigaev, S.Y. Stefanovich, P.D. Sarkisov, E.V. Lopatina, Mater. Sci. Eng. B 32 (1995) 17.
- [5] J.J. Shyu, J.R. Wang, J. Am. Ceram. Soc. 83 (2000) 3135.
- [6] N.S. Prasad, K.B.R. Varma, Y. Takahashi, Y. Benino, T. Fujiwara, T. Komatsu, J. Solid State Chem. 173 (2003) 209.
- [7] G. Boyd, R. Miller, K. Nassau, W. Bond, A. Savage, Appl. Phys. Lett. 5 (1964) 234.
- [8] G. Peterson, A. Ballman, P. Lenzo, M. Bridenbaugh, Appl. Phys. Lett. 5 (1964) 62.
- [9] R. Magnusson, T.K. Gaylord, Appl. Opt. 13 (1974) 1545.
- [10] M.M. Abouelleil, F.J. Leonberger, J. Am. Ceram. Soc. 72 (1989) 1311.
- [11] M. Imaoka, T. Yamazaki, J. Ceram. Soc. Jpn. 76 (1968) 160.
- [12] K. Nassau, C.A. Wang, M. Grasso, J. Am. Ceram. Soc. 62 (1979) 503.
- [13] H.G. Kim, T. Komatsu, R. Sato, K. Matusita, J. Non-Cryst. Solids 162 (1993) 201.
- [14] M.V. Shankar, K.B.R. Varma, J. Non-Cryst. Solids 243 (1999) 192.
- [15] Y. Hu, C.L. Huang, J. Non-Cryst. Solids 278 (2000) 170.
- [16] M. Todorovic, Lj. Radonjić, Ceram. Int. 23 (1997) 55.
- [17] JCPDS-International center for diffraction data, 20-0631.
- [18] JCPDS-International center for diffraction data, 36-0307.
- [19] N.S. Prasad, K.B.R. Varma, J. Am. Ceram. Soc. 88 (2) (2005) 357.
- [20] H.G. Kim, T. Komatsu, R. Sato, K. Matusita, J. Mater. Sci. 31 (1996) 2159.
- [21] M. Tomozawa, R.H. Doremus, Treatise on Materials Science and Technology, vol. 12, Academic press, 1977, p. 296.
- [22] G.S. Murugan, K.B.R. Varma, Ferroelectrics 266 (2002) 259.
- [23] J.M. Stevels, Handbuch der physik 20 (1957) 372.
- [24] H.E. Taylor, J. Soc. Glass Technol. 41 (1957) 350T; H.E. Taylor, J. Soc. Glass Technol. 43 (1959) 124T.
- [25] K.J. Charles, J. Appl. Phys. 32 (1961) 1115.
- [26] S.R. Elliott, Solid State Ionics 27 (1988) 131.
- [27] A. Doi, Phys. Chem. Glasses 33 (1992) 184.
- [28] S. Lanfredi, A.C.M. Rodrigues, J. Appl. Phys. 86 (1999) 2215.
- [29] M.H. Lewis, Glasses and Glass-ceramics, Chapman and Hall, 1989, p. 123.
- [30] H.D. Megaw, Acta Crystallogr. 7 (1954) 187.
- [31] J.W. Cha, J.B. Kim, C.S. Kim, J.N. Kim, Ferroelectrics Lett. 17 (1994) 111.